Theoretical and Experimental Investigation of a Thermoelectric Cooler for Marine Cooling Systems

Andrii Bukaros[1], Oleg Onishchenko[2], Leonid Hordishevskyi[1], Liliia Lebedieva[1], Valeriia Bukaros[1]

The analysis of literary sources show that thermoelectric devices are used in marine transport as electrical power generators and coolers. Both applications require determination of the Peltier elements dynamic properties. Known dynamic models of thermoelectric devices are relatively complicated and do not take into account the inertia of thermoelectric processes. To overcome this contradiction, in this paper, a simulation model of the Peltier element based on the one-dimensional heat conduction equation and the integral Laplace transform have been synthesised. This model consists of elementary transfer functions and establishes a relationship between cold and hot junction temperatures and an electrical current. The experiment has been conducted to verify the obtained model. During the experiment, the temperatures of the thermoelectric cooler hot and cold surfaces have been measured at different values of the load current. A comparison of the experimental investigation results with the results of numerical simulation in the Matlab/Simulink software environment has been carried out. This comparison shows the convergence of the experimental and model time dependences of the thermoelectric cooler hot and cold surfaces temperatures with an error not exceeding 5%. Thus, the functionality of the synthesised model has been experimentally confirmed. The simplicity and clarity of the proposed model makes it quite easy to build and adjust the parameters of thermoelectric marine cooling systems. Further improvement of the model is possible by considering the temperature dependence of thermoelectric parameters and the Thompson effect.

KEYWORDS
~ Cold surface temperature
~ Experimental investigation
~ Hot surface temperature
~ Peltier element
~ Simulation model
~ Thermoelectric device
~ Transfer function

[1] Odesa Military Academy, Faculty of Missile and Artillery Weapons, Odesa, Ukraine
[2] National University "Odessa Maritime Academy", Faculty of Marine Mechanics, Odesa, Ukraine
e-mail: andrey.bucaros@gmail.com
doi: 10.7225/toms.v14.n01.003

Received: 15 Oct 2023 / Revised: 14 May 2024 / Accepted: 8 Mar 2025 / Published: 20 Apr 2025

1. INTRODUCTION

The problem of shortage and rational use of energy resources is currently very relevant both in the world and, in particular, in marine transport. The application of thermoelectric phenomena: the Seebeck effect, which is used in thermoelectric generators to convert thermal energy into electrical energy, and the Peltier effect applied in thermoelectric converters to transform electrical energy into thermal energy, can be a promising way to solve this problem.

Thermoelectric generators are used in marine transport mainly to convert the waste heat of exhaust gases into electricity. As the analysis of literary sources shows, this direction arouses unabated interest from researchers. In particular, (Konstantinou et al., 2022**;** Saha et al., 2023) note that marine internal combustion engines emit more than 50% of the produced energy into the atmosphere with exhaust gases. Firstly, this leads to significant environmental pollution and increases the negative impact of the greenhouse effect. Secondly, it reduces the overall efficiency of the propulsion system. Authors (Patil et al., 2018**;** Alghoul et al., 2018**;** Fernández-Yáñez et al., 2021) prove that thermoelectric generators have the following advantages compared to other means (Farhat et al., 2022) of exhaust gas thermal energy recovery: environmental friendliness, absence of noise, vibration and working fluids, high reliability, low operating costs, etc.

In recent years, thermoelectric converters (Peltier elements) have become widespread in marine cooling systems, such as fishermen's vessel cold storage systems (Rahman et al., 2019), naval vessel radar refrigeration systems (Yim et al., 2020), research vessel deep-sea water sampler cooling systems (Wu et al., 2022). The authors mentioned above note that the use of thermoelectric coolers (TEC) in marine cooling systems has such advantages over vapour compression refrigeration units (Bukaros et al., 2023**;** Onishchenko et al., 2023) as the absence of refrigerants emissions into the atmosphere, reduction in fuel consumption, long service life, low inertia, and a wide range of Peltier elements operating temperatures.

The considered marine systems, in particular, thermoelectric temperature stabilisation systems, necessarily provide for automatic control of the TEC performance, which is impossible without knowledge of the Peltier elements dynamic properties. However, as the analysis of literary sources shows, the known TEC dynamic models (Kotsur, 2015**;** Ji et al., 2016**;** Bukaros and Onishchenko, 2023**;** Piggott, 2019**;** MathWorks, 2023) are too overloaded, do not take into account the inertia of thermoelectric processes, the heat exchange of the TEC hot surface with the environment and are unsuitable for the synthesis of classical proportional-integral-derivative temperature controllers (Kiam et al., 2005).

Until now there have been no sufficiently simple mathematical models that describe the dynamic properties of thermoelectric coolers and could be easily implemented in simulation environments. At the same time, such models are in demand for the construction of marine cooling systems. In order to resolve this contradiction, a simulation dynamic model built on the basis of elementary transfer functions describing the main thermoelectric processes of the Peltier element is proposed in this paper.

2. THEORETICAL INVESTIGATION OF THE THERMOELECTRIC COOLER

In the general case, the TEC shown in Figure 1 consists of Peltier elements, which are connected in series to the electric current flow and in parallel to the heat flow. Each of the Peltier elements consists of two n-type and p-type semiconductor rods. One end of these rods (hot junction) is supplied with a voltage with the polarity shown in Figure 1, other ends are electrically connected (cold junction). When changing the direction of current flow, the hot and cold junctions change places.

To simplify the theoretical description of the thermoelectric processes taking place in TEC, a one-dimensional model of the Peltier element, consisting of two homogeneous rods with length l and cross-sectional area A, will be considered. Since the electrical, thermal, and thermoelectric parameters of n- and p-type rods are close in value (Witting et al., 2019), the volumetric heat capacity c, thermal conductivity k, specific resistance ρ and Seebeck coefficient α of both rods are considered to be the same and equal to the average value. According to the accepted one-dimensional model, heat removal from the side surfaces of the Peltier element is absent. In this paper, the heat exchange of a cold and hot surface (joint) with the environment will be considered according to Newton's law with heat transfer coefficients h_l and h_0, respectively, but without additional heat load q_l (q_0). The points of Peltier elements connection with working surfaces and insulating plates are considered objects with concentrated parameters, therefore, their temperature does not depend on the x coordinate. The temperature dependences of the Peltier element electrical, thermal, and thermoelectric parameters, as well as the Thompson effect (Piggott, 2019), are neglected.

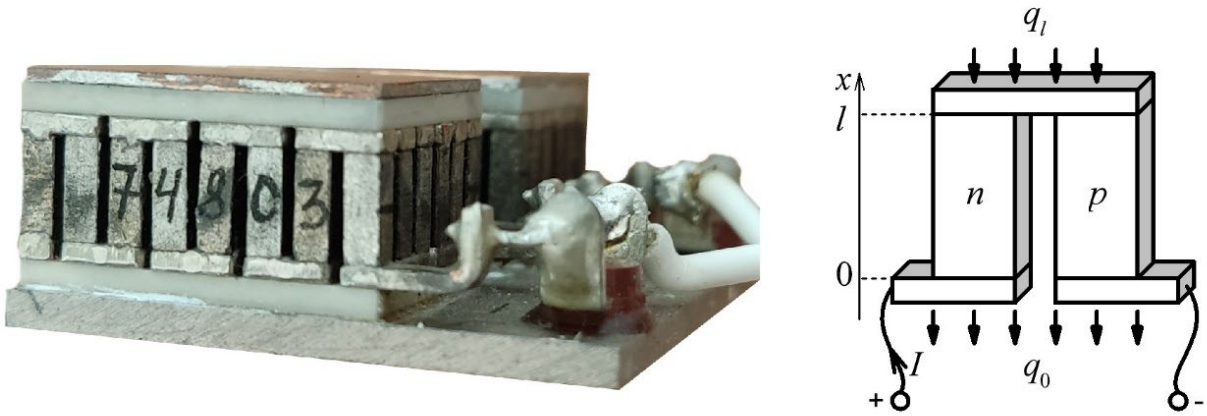

Figure 1. Thermoelectric cooler and Peltier element.

The given assumptions make it possible to write the equation of the Peltier element thermal conductivity in the following form (Yang et al., 2005):

$$c \cdot \frac{\partial T(x,t)}{\partial t} = k \cdot \frac{\partial^2 T(x,t)}{\partial x^2} + \rho \cdot \left(\frac{I(t)}{A}\right)^2 \quad \text{.....(1)}$$

with the initial condition:

$$T(x,0) = T_a \quad \text{.....(2)}$$

where T is the material temperature of the Peltier element, K; T_a is the ambient temperature, K; I is the current, A; t is the time, s; c is the volume thermal conductivity of the rod, J/(cm^3·K); k is the thermal conductivity of the rod, W/(cm·K), ρ is the specific resistance of the rod, Ohm·cm, x is the coordinate directed along the length of the rod, cm; while A is the cross-sectional area of the rod, cm^2.

The boundary conditions for equation (1) will have the following form:

- for a hot junction:

$$k \cdot A \cdot \frac{\partial T(x,t)}{\partial x} + \alpha \cdot T(0,t) \cdot I(t) + \frac{r_0}{A} \cdot I^2(t) - h_0 \cdot A \cdot [T(0,t) - T_a] = c_0 \cdot \frac{\partial T(0,t)}{\partial t} \quad \text{.....(3)}$$

- for a cold junction:

$$-k \cdot A \cdot \frac{\partial T(x,t)}{\partial x} - \alpha \cdot T(l,t) \cdot I(t) + \frac{r_l}{A} \cdot I^2(t) + h_l \cdot A \cdot [T_a - T(l,t)] = c_l \cdot \frac{\partial T(l,t)}{\partial t} \quad \text{.....(4)}$$

where c_l, c_0 is the insulation plate heat capacity of the cold and hot junctions, respectively, J/K; r_l, r_0 is the specific contact resistance of cold and hot junctions, respectively, Ohm·cm^2; h_l, h_0 is the convective heat transfer coefficient of cold and hot surfaces, respectively, W/(cm^2·K); α is the Seebeck coefficient, V/K; l is the length of the rod in cm.

To solve the equation (1) with initial condition (2) and boundary conditions (3), (4) the integral Laplace transform has been applied:

$$\frac{\partial^2 T(x,s)}{\partial x^2} - \frac{c}{k} \cdot (s \cdot T(x,s) - T_a) + \frac{\rho}{k \cdot A^2} \cdot I^2(s) = 0 \quad \text{.....(5)}$$

$$T(x,0) = T_a \quad \text{.....(6)}$$

$$\frac{\partial T(0,s)}{\partial x} + \frac{1}{k}\left[\frac{\alpha}{A} \cdot T(0,s) \cdot I(s) + \frac{r_0}{A^2} \cdot I^2(s) - h_0 \cdot [T(0,s) - T_a] - \frac{c_0}{A} \cdot (s \cdot T(0,s) - T_a)\right] = 0 \quad \text{.....(7)}$$

$$\frac{\partial T(l,s)}{\partial x} + \frac{1}{k}\left[\frac{\alpha}{A} \cdot T(l,s) \cdot I(s) - \frac{r_l}{A^2} \cdot I^2(s) - h_l \cdot [T_a - T(l,s)] + \frac{c_l}{A} \cdot (s \cdot T(l,s) - T_a)\right] = 0 \quad \text{.....(8)}$$

where s is the Laplace variable.

The general solution of equation (5) has the form:

$$T(x,s) = C_1 \cdot e^{x\sqrt{c\cdot s/k}} + C_2 \cdot e^{-x\sqrt{c\cdot s/k}} + \frac{\rho}{s\cdot c\cdot A^2}\cdot I^2(s) + \frac{T_a}{s} \quad \text{.....(9)}$$

To find an expression for the hot or cold junction temperature, the constants C_1 and C_2 are substituted into the corresponding boundary condition (7) or (8) and the equation (9) with the coordinate x corresponding to the opposite junction. As a result, a system of equations is solved relative to the constants C_1 and C_2, after which the obtained values are substituted into the general solution (9). Thus, the partial solutions of equation (5) for hot and cold junction temperatures take the form:

$$T(0,s) = \left[\rho - \frac{\rho}{cosh(y)} + \frac{y\cdot r_0}{l\cdot coth(y)}\right]\frac{I^2(s)}{s\cdot c\cdot A^2} + \frac{cosh(y)-1}{cosh(y)}\cdot\frac{T_a}{s} + \frac{T(l,s)}{cosh(y)} - \frac{c_0\cdot[s\cdot T(0,s)-T_a]-\alpha\cdot T(0,s)\cdot I(s)-h\cdot A\cdot[T_a-T(0,s)]}{k\cdot A\cdot y/l\cdot coth(y)} \quad \text{...(10)}$$

$$T(l,s) = \left[\rho - \frac{\rho}{cosh(y)} + \frac{y\cdot r_l}{l\cdot coth(y)}\right]\frac{I^2(s)}{s\cdot c\cdot A^2} + \frac{cosh(y)-1}{cosh(y)}\cdot\frac{T_a}{s} + \frac{T(0,s)}{cosh(y)} - \frac{c_l\cdot[s\cdot T(l,s)-T_a]+\alpha\cdot T(l,s)\cdot I(s)-h\cdot A\cdot[T_a-T(l,s)]}{k\cdot A\cdot y/l\cdot coth(y)} \quad \text{.....(11)}$$

where $y = l\sqrt{c\cdot s/k}$.

As can be seen, expressions (10) and (11) contain hyperbolic cosine and cotangent functions, which can be expanded into power series, and if we limit ourselves to the first two terms of the series, the expansion error will not exceed 4%. Therefore, by substituting the decomposed hyperbolic functions into expressions (10) and (11), after elementary transformations, partial solutions of equation (5) have been finally obtained:

$$T(0,s) = \frac{(\tau_J\cdot K_{J0}^{'}\cdot s+K_{J0})\cdot I^2(s)}{(\tau_J\cdot s+1)(\tau_{P0}\cdot s+1)} + \frac{K_P\cdot T(0,s)\cdot I(s)}{\tau_{P0}\cdot s+1} + \frac{K_{T0}\cdot[T_a-T(0,s)]}{\tau_{P0}\cdot s+1} + \frac{(\tau_P\cdot s+1)\cdot T(l,s)}{(\tau_J\cdot s+1)(\tau_{P0}\cdot s+1)} + \frac{\tau_J\cdot\tau_{P0}\cdot s^2+\tau_{P0}\cdot s}{(\tau_J\cdot s+1)(\tau_{P0}\cdot s+1)}\cdot T_a \quad \text{.....(12)}$$

$$T(l,s) = \frac{(\tau_J\cdot K_{Jl}^{'}\cdot s+K_{Jl})\cdot I^2(s)}{(\tau_J\cdot s+1)(\tau_{Pl}\cdot s+1)} - \frac{K_P\cdot T(l,s)\cdot I(s)}{\tau_{Pl}\cdot s+1} + \frac{K_{Tl}\cdot[T_a-T(l,s)]}{\tau_{Pl}\cdot s+1} + \frac{(\tau_P\cdot s+1)\cdot T(l,s)}{(\tau_J\cdot s+1)(\tau_{Pl}\cdot s+1)} + \frac{\tau_J\cdot\tau_{Pl}\cdot s^2+\tau_{Pl}\cdot s}{(\tau_J\cdot s+1)(\tau_{Pl}\cdot s+1)}\cdot T_a \quad \text{.....(13)}$$

with the transfer coefficients and time constants:

$$K_{J0,l} = \frac{l\cdot(\rho\cdot l+2r_{0,l})}{2\cdot k\cdot A^2} = \frac{R+2R_{0,l}}{2\cdot K},\quad K_{J0,l}^{'} = \frac{l\cdot(\rho\cdot l+3r_{0,l})}{3\cdot k\cdot A^2} = \frac{R+3R_{0,l}}{3\cdot K},\quad K_{T0.l} = \frac{h_{0,l}\cdot l}{k},\quad K_P = \frac{\alpha\cdot l}{k\cdot A} = \frac{\alpha}{K} \quad \text{.....(14)}$$

$$\tau_J = \frac{c\cdot l^2}{2\cdot k} = \frac{C}{2\cdot K},\quad \tau_P = \frac{c\cdot l^2}{3\cdot k} = \frac{C}{3\cdot K},\quad \tau_{p0,l} = \frac{c\cdot l^2}{3\cdot k} + \frac{c_{0,l}\cdot l}{k\cdot A} = \frac{C}{3\cdot K} + \frac{c_{0,l}}{K} \quad \text{.....(15)}$$

where $R_{0,l}$ is the electrical resistance of the hot (cold) junction, respectively, Ohm; C is the heat capacity of the Peltier element rod, J/K; K is the thermal conductivity of the Peltier element rod, W/K.

In expressions (12), (13), the first term describes the release of Joule heat in the volume of the Peltier element rod and in the contact resistance of the hot (cold) junction, the second term describes the Peltier heat absorption, the third term describes the heat exchange of the hot (cold) surface with the environment, the fourth term describes heat transfer according to the Fourier law, and the fifth term takes into account non-zero initial conditions.

The obtained equations (12) and (13) make it possible to build a relatively simple simulation model of the Peltier element, the structural diagram of which is shown in Figure 2. As can be seen, the obtained model consists of five elementary transfer functions, each of which describes a separate thermal process occurring in the Peltier element in accordance with (12), (13).

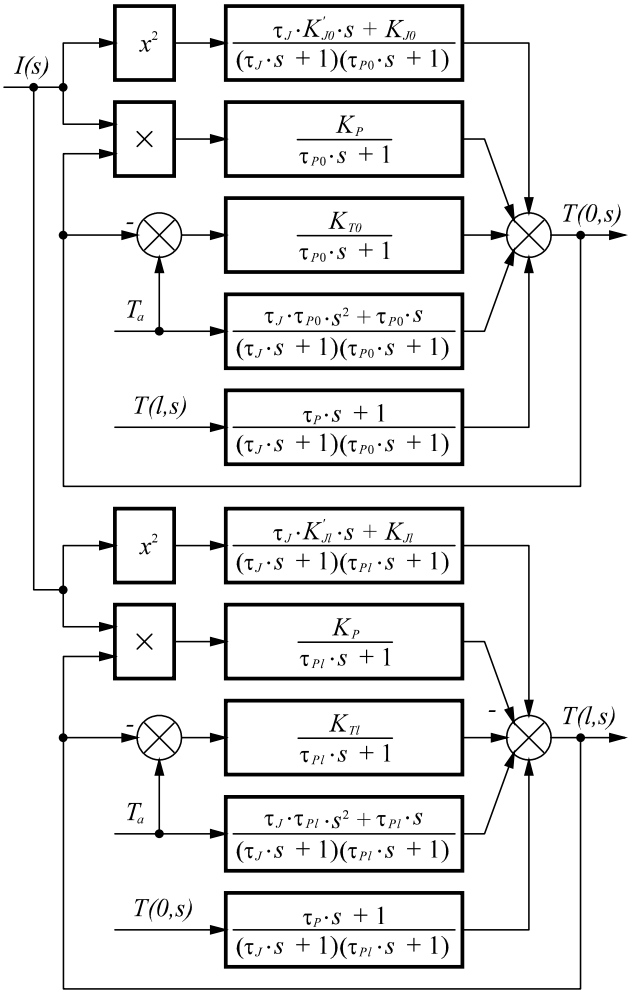

Figure 2. Structural diagram of the Peltier element simulation model.

Since the same current flows through all Peltier elements in the TEC, and all hot and cold junctions are connected by isothermal surfaces, the obtained simulation model is also used to describe the processes taking place in the TEC.

3. EXPERIMENTAL INVESTIGATION OF THE THERMOELECTRIC COOLER

To verify the simulation model, an experimental unit, the appearance of which is shown in Figure 3, has been assembled.

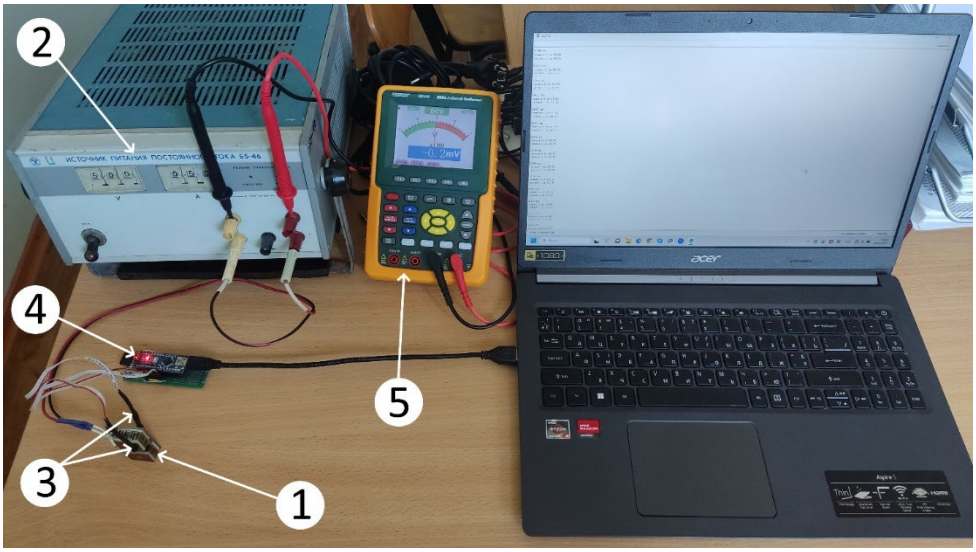

Figure 3. Experimental unit for researching the TEC dynamic properties.

Figure 3 shows: 1 – TEMO-3 thermoelectric cooler; 2 – B5-46 direct current power supply unit; 3 – DS18B20 digital temperature sensors; 4 – Arduino Nano module based on ATmega328P-AU microcontroller; 5 – Extech MS420 two-channel digital oscilloscope.

The main characteristics of the used equipment and devices are as follows:

1. TEMO-3 thermoelectric cooler – permissible temperature difference of hot and cold surfaces is 62 K, characteristic current is 3,5 A, maximum cooling capacity is 4,5 W, resistance to alternating current flow is 0,68 Ohm, the time to set working values of parameters is 10 min;
2. B5-46 direct current power supply unit – output voltage is 0,01-9,99 V, load current is 0,01-4,99 A, voltage setting discreteness is 10 mV, current setting discreteness is 10 mA, voltage error is 0,5 %, current error is 1%;
3. DS18B20 digital temperature sensors – range of measured temperatures, if from -55 °C to +125 °C, the absolute error is ±0,5 °C, programmable resolution ranges from 9 to 12 bits;
4. ATmega328P-AU microcontroller – bit depth is 8 bit, frequency is 20 MHz;
5. Extech MS420 digital oscilloscope – bandwidth is 20 MHz, range of measured voltages is 0-400 V, range of measured currents is 0-20 A.

The TEMO-3 thermoelectric cooler used in the experiment consists of 96 Peltier elements made of material based on bismuth telluride with geometric dimensions: length l = 0,55 cm, cross-sectional area A = 0,037 cm^2 and thermoelectric parameters (Witting et al., 2019): volume heat capacity c = 1,4 J/(cm^3·K), thermal conductivity k = 0,0189 W/(cm·K), specific resistance ρ = 0,0016 Ohm·cm, Seebeck coefficient α = 230·10^{-6} V/K.

Taking into account the different geometries of insulating ceramic and heat-emitting copper plates, their total heat capacity in terms of one Peltier element is c_0 = 0,276 J/K and c_l = 0,124 J/K for hot and cold surfaces, respectively.

During the experiment, the TEC has been installed on the side face, as shown in Figure 3, to ensure the same conditions for convective heat removal from hot and cold surfaces. At the same time, the convective heat transfer coefficients, calculated according to the method proposed by (Churchill and Chu, 1975) have been h_0 = 0,0128 W/(cm^2·K) and h_l = 0,0182 W/(cm^2·K), respectively.

The value of the hot and cold junction specific contact resistance is assumed to be the same and equal to $r_0 = r_l$ = 5·10^{-6} Ω·cm^2.

During the experiment, the ambient temperature has been kept constant and equal to T_a = 22 °C.

At the first stage of the experiment, a load current of 0,5 A has been set using the B5-46 power supply unit. The ATmega328P-AU microcontroller has been switched to data transmission mode on the virtual COM port. With the help of the Arduino IDE software, the temperature values of the hot and cold surfaces have been recorded from the DS18B20 sensors for 25 minutes. Then the power supply of the experimental unit was turned off for 1 hour to bring the TEC parameters to their initial state.

At the second stage of the experiment, a load current of 1 A was set, after which the sequence of the first stage actions was repeated. In order to increase the results reliability and exclude possible systematic errors, the experiment has been performed three times at each stage, with the temperature sensors changing places.

4. RESULTS

The results of the experiment are shown by circles in Figures 4 and 5. In the same figures, solid lines show the results of the TEC hot and cold surfaces temperature numerical simulation according to equations (12), (13) in the Matlab/Simulink environment.

Analysis of Figure 4 shows a high level of coincidence of model time temperature dependence curves and experimental results at a load current of 0.5 A. The maximum discrepancy between experimental and model data for the TEC hot and cold surfaces temperature does not exceed 0,75 °C or 4,5%.

A slightly different picture is observed in Figure 5, when the TEC is fed with a current of 1 A. The time dependences of the TEC cold surface temperature obtained in the model (lower black solid curve in Figure 5) and experimentally show good agreement. The maximum discrepancy occurs only at the beginning of the curve and does not exceed 1,25 °C or 5%. At the same time, the maximum discrepancy of the TEC hot surface temperature model curve (the upper black solid curve in Figure 5) with the experimental data is visible to the naked eye and is 2,6 °C or 3,6%. The relative value of this discrepancy

in percentage remains almost constant over the entire time range, and its absolute expression increases with the increase in the temperature of the hot surface.

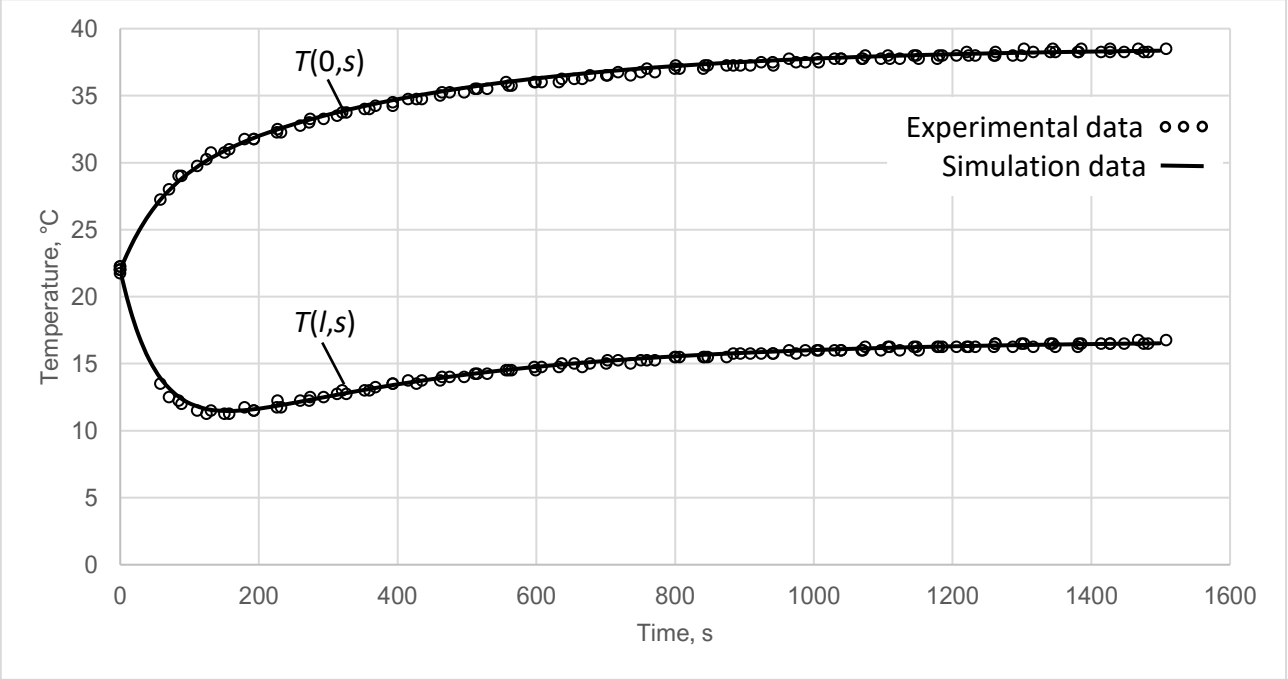

Figure 4. Time dependences of the TEC hot and cold surface temperature at current of 0.5 A.

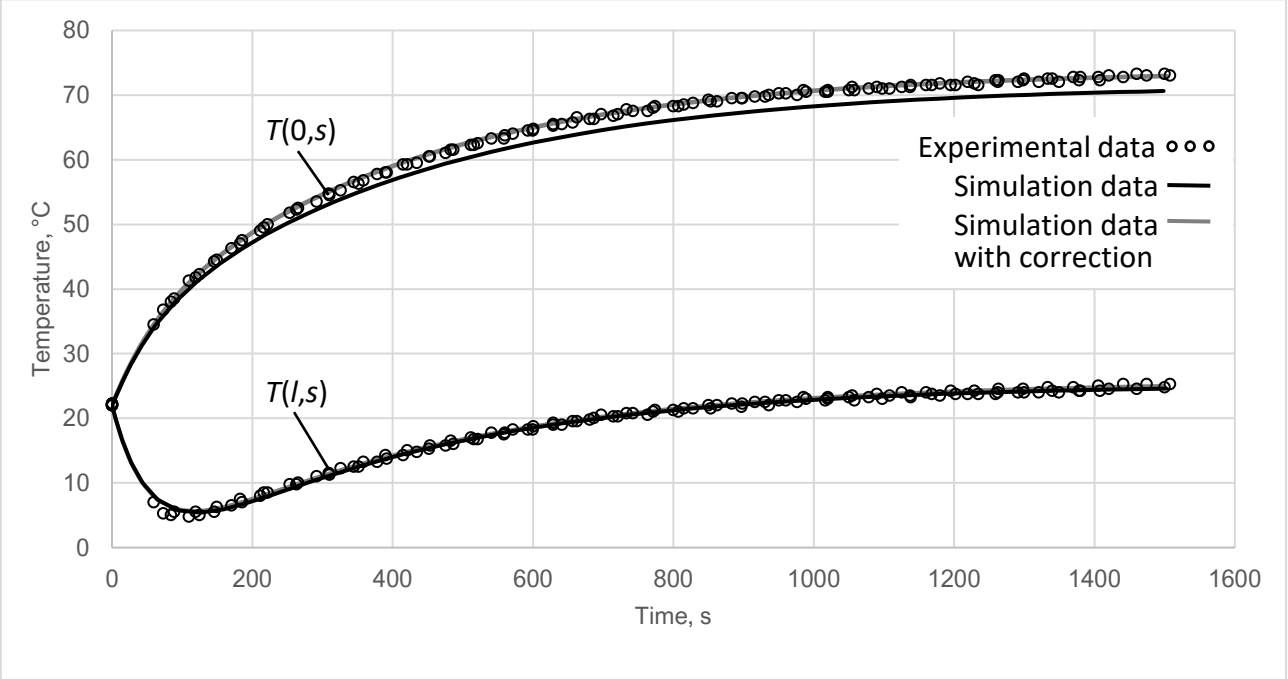

Figure 5. Time dependences of the TEC hot and cold surface temperature at current of 0.5 A.

5. DISCUSSION AND CONCLUSIONS

The nature of the discrepancy that is observed in Figure 5 indicates either the presence of a multiplicative error in measuring the TEC hot surface temperature, or the imperfection of the model. The first remark is excluded by the experiment conditions. In particular, the experiment was performed three times with the same environmental conditions, while the hot and cold surfaces temperature sensors were changed. The second remark is quite valid, since the TEC model does not take into account the temperature dependence of the Peltier elements parameters. Since the temperature of the hot surface at a current of 1 A exceeds the similar temperature at a current of 0,5 A by almost two times, then, as (Witting et al., 2019) show, the TEC parameters also undergo significant changes.

Thus a correction of the Peltier elements parameters has been carried out, taking into account the increased temperature of the hot and cold surface at the second stage of the experiment when TEC was supplied with a current of 1 A. The adjusted values of the parameters, in accordance with (Witting et al., 2019), are: specific resistance ρ = 0,0018 Ω·cm, thermal conductivity k = 0,0174 W/(cm·K). The convective heat transfer coefficients of the TEC hot and cold surfaces, calculated according to the method of (Churchill and Chu, 1975), have also been adjusted and were h_0 = 0,0134 W/(cm^2·K) and h_l = 0,0191 W/(cm^2·K), respectively.

The results of simulation with adjusted TEC parameters are shown in Figure 5 by grey solid curves. As can be seen, the corrected TEC hot surface temperature model curve (the upper grey solid curve in Figure 5) is very accurately superimposed on the experimental results, the discrepancy not exceeding 0,75 °C or 1%, and there is no multiplicative error. The corrected TEC cold surface temperature model curve (lower grey solid curve in Figure 5) practically overlaps the previously obtained curve. It can be noted that taking into account the influence of the hot and cold surface temperature on the TEC thermoelectric parameters can increase the accuracy of the model by 2.6%.

Thereby, the obtained simulation results and the value of the maximum discrepancy of 5% in comparison with the experimental data testify to the efficiency of the proposed TEC simulation model. Time dependences of the TEMO-3 hot and cold surface temperature have been obtained for the first time. The resulting model in Figure 2, in contrast to the known analogues (Kotsur, 2015**;** Piggott, 2019), is much simpler and consists of elementary transfer functions. Unlike the well-known models (Ji et al., 2016**;** Bukaros and Onishchenko, 2023**;** MathWorks, 2023), the proposed one describes the dynamics of the main thermoelectric processes, and also takes into account the heat capacity of the insulating plates, the heat release in the contact resistance, and the heat exchange of the TEC hot surface with the environment. The simplicity of the model makes it easy to calculate and optimise the setting parameters of marine cooling systems based on TEC.

It seems obvious that the accuracy of the considered model will decrease with increasing load current and hot and cold surface temperatures. Therefore, in future research it is important to improve the model, taking into account the temperature dependences of the TEC thermoelectric parameters, as well as the Thomson effect and additional heat load from the cooled object.

CONFLICT OF INTEREST

The authors declare no conflict of interest.

REFERENCES

Alghoul, M.A., Shahahmadi, S.A., Yeganeh, B., Asim, N., Elbreki, A.M., Sopian, K.B., Tiong, S.K. and Amin, N. (2018) 'A review of thermoelectric power generation systems: Roles of existing test rigs/prototypes and their associated cooling units on output performance', Energy Conversion and Management, 174, pp. 138–156. Available at: https://doi.org/10.1016/j.enconman.2018.08.019.

Bukaros, A., Onishchenko, O., Herega, A., Trushkov, H. and Konkov, K. (2023) 'Simulation modeling of vapor compression refrigeration unit temperature modes', in Zaporozhets, A. (ed.) Systems, Decision and Control in Energy IV. Studies in Systems, Decision and Control, 454. Switzerland: Springer, pp. 253–266. Available at: https://doi.org/10.1007/978-3-031-22464-5_14.

Bukaros, A. and Onishchenko, O. (2023) 'Simulation of thermoelectric coolers for automotive temperature stabilization systems', in Prentkovskis, O., Yatskiv (Jackiva), I., Skačkauskas, P., Karpenko, M. and Stosiak, M. (eds) TRANSBALTICA XIV: Transportation Science and Technology. TRANSBALTICA 2023. Lecture Notes in Intelligent Transportation and Infrastructure. Switzerland: Springer. Available at: https://doi.org/10.1007/978-3-031-52652-7_11.

Churchill, S.W. and Chu, H.H.S. (1975) 'Correlating equations for laminar and turbulent free convection from a vertical plate', International Journal of Heat and Mass Transfer, 18(11), pp. 1323–1329. Available at: https://doi.org/10.1016/0017-9310(75)90243-4.

Farhat, O., Faraj, J., Hachem, F., Castelain, C. and Khaled, M. (2022) 'A recent review on waste heat recovery methodologies and applications: Comprehensive review, critical analysis and potential recommendations', Cleaner Engineering and Technology, 6, p. 100387. Available at: https://doi.org/10.1016/j.clet.2021.100387.

Fernández-Yáñez, P., Romero, V., Armas, O. and Cerretti, G. (2021) 'Thermal management of thermoelectric generators for waste energy recovery', Applied Thermal Engineering, 196, p. 117291. Available at: https://doi.org/10.1016/j.applthermaleng.2021.117291.

Ji, D., Tseng, K.J., Wei, Z., Zheng, Y. and Romagnoli, A. (2016) 'A simulation study on a thermoelectric generator for waste heat recovery from a marine engine', Journal of Electronic Materials, 46(5), pp. 2908–2914. Available at: https://doi.org/10.1007/s11664-016-5038-8.

Kiam, H.A., Chong, G. and Li, Y. (2005) 'PID control system analysis, design, and technology', IEEE Transactions on Control Systems Technology, 13(4), pp. 559–576. Available at: https://doi.org/10.1109/tcst.2005.847331.

Konstantinou, G., Kyratsi, T. and Louca, L.S. (2022) 'Design of a thermoelectric device for power generation through waste heat recovery from marine internal combustion engines', Energies, 15(11), p. 4075. Available at: https://doi.org/10.3390/en15114075.

Kotsur, M. (2015) 'Optimal control of distributed parameter systems with application to transient thermoelectric cooling', Advances in Electrical and Computer Engineering, 15(2), pp. 117–122. Available at: https://doi.org/10.4316/aece.2015.02015.

MathWorks (n.d.) Peltier Device. Available at: https://www.mathworks.com/help/sps/ref/peltierdevice.html (Accessed: 12 October 2023).

Onishchenko, O., Bukaros, A., Melnyk, O., Yarovenko, V., Voloshyn, A. and Lohinov, O. (2023) 'Ship refrigeration system operating cycle efficiency assessment and identification of ways to reduce energy consumption of maritime transport', in Zaporozhets, A. (ed.) Systems, Decision and Control in Energy V. Studies in Systems, Decision and Control, 481. Switzerland: Springer, pp. 641–652. Available at: https://doi.org/10.1007/978-3-031-35088-7_36.

Patil, D., Arakerimath, R.R., Twelftree, J. and Hulston, C. (2018) 'Thermoelectric materials and heat exchangers for power generation – A review', Renewable and Sustainable Energy Reviews, 95, pp. 1–22. Available at: http://dx.doi.org/10.1016/j.rser.2018.07.003.

Piggott, A. (2019) 'Detailed transient multiphysics model for fast and accurate design, simulation and optimization of a thermoelectric generator (TEG) or thermal energy harvesting device', Journal of Electronic Materials, 48(9), pp. 5442–5452. Available at: https://doi.org/10.1007/s11664-019-06952-x.

Rahman, M.A., Widyatama, A., Majid, A.I. and Suhanan, S. (2019) 'Peltier thermoelectric refrigeration system as the future cold storage system for Indonesia: A review', in Proc. 5th International Conference on Science and Technology, Yogyakarta, Indonesia, 30–31 July, pp. 540–545. Available at: https://doi.org/10.1109/icst47872.2019.9166392.

Saha, M., Tregenza, O., Twelftree, J. and Hulston, C. (2023) 'A review of thermoelectric generators for waste heat recovery in marine applications', Sustainable Energy Technologies and Assessments, 59, p. 103394. Available at: https://doi.org/10.1016/j.seta.2023.103394.

Witting, I.T., Chasapis, T.C., Ricci, F., Peters, M., Heinz, N.A., Hautier, G. and Snyder, G.J. (2019) 'The thermoelectric properties of bismuth telluride', Advanced Electronic Materials, 5(6), p. 1800904. Available at: https://doi.org/10.1002/aelm.201800904.

Wu, S.-J., Wang, X., Wang, S., Zhang, B., Yang, C.-J. and Zhi, H. (2022) 'Active temperature-preserving deep-sea water sampler configured with a pressure-adaptive thermoelectric cooler module', Deep Sea Research Part I: Oceanographic Research Papers, 181, p. 103701. Available at: https://doi.org/10.1016/j.dsr.2022.103701.

Yang, R., Chen, G., Ravi Kumar, A., Snyder, G.J. and Fleurial, J.-P. (2005) 'Transient cooling of thermoelectric coolers and its applications for microdevices', Energy Conversion and Management, 46(9–10), pp. 1407–1421. Available at: https://doi.org/10.1016/j.enconman.2004.07.004.

Yim, S.-W., Lee, D.-K., Kim, H.-T., Ra, Y.-E., Kim, H., Park, G. and Kim, W. (2020) 'Numerical analysis of active refrigeration performance in thermoelectric device integrated with naval vessel radar system', Transactions of the Korean Society of Mechanical Engineers, 44(7), pp. 415–421. Available at: https://doi.org/10.3795/ksme-b.2020.44.7.415.